Calderon, J. C., Celorrio, V., Nieto-Monge, M. J., Fermin, D., Pardo, J. I., Moliner, R., & Lazaro, M. J. (2016). Palladium–nickel materials as cathode electrocatalysts for alkaline fuel cells. *International Journal of Hydrogen Energy*, *41*(47), 22538–22546. https://doi.org/10.1016/j.ijhydene.2016.08.192

Palladium-Nickel Materials as Cathode Electrocatalysts for Alkaline Fuel Cells

J.C. Calderón[a, †], V. Celorrio[b, †], M.J. Nieto-Monge[a], D.J. Fermín[b], J.I. Pardo[c], R. Moliner[a], M.J. Lázaro[a]*

[a]Instituto de Carboquímica (CSIC), Miguel Luesma Castán 4, 50018, Zaragoza, Spain

[b]School of Chemistry, University of Bristol, Cantocks Close, BS8 1TS, Bristol, United Kingdom

[c]Instituto Universitario de Investigación de Ingeniería de Aragón (I3A), Mariano Esquillor s/n, 50018, Zaragoza, Spain

[†]*These authors contributed equally to this work.*

**Corresponding author email address: mlazaro@icb.csic.es*

ABSTRACT

In this work, Pd-Ni catalysts supported on carbon nanofibers were synthesized, with metal contents and Pd:Ni atomic ratios close to 25 wt. % and 1:2, respectively. Previously, the carbon nanofibers were chemically treated, in order to create surface oxygen and/or nitrogen groups. The synthesized catalysts displayed low crystallinity degree and high dispersion on carbon supports, especially in those with surface functional groups. Oxygen reduction reaction (ORR) was studied by rotating ring-disk electrode (RRDE) techniques. When the kinetic current is normalized by the mass of Pd present in the electrode, higher activities were obtained for the synthesized materials in comparison with the activity observed for a commercial Pd/C E-TEK catalyst. Some differences are reported for the different materials under study, mainly dependent on the presence of oxygen surface groups on the carbon support. In light of the results, we can propose the synthesized catalysts as possible candidates for cathodes in alkaline direct methanol fuel cells.

Keywords: Pd-Ni catalysts; alkaline medium; oxygen reduction; carbon nanofibers; hydrogen peroxide production.

1. INTRODUCTION

Polymer electrolyte membrane fuel cells (PEMFCs) have been postulated as possible alternatives in the production of electricity for portable and stationary applications, due to their advantageous characteristics such as low working temperature, high energy conversion efficiency, high power density, low or zero pollution emissions, quick start-up and long lifetime [1]. Several works in the literature predicted that PEMFCs could develop similar efficiencies to batteries, internal combustion engines and/or power grids [2]. However, the implement of this technology still must confront challenges related to technical details such as the low kinetics in the oxygen reduction reaction (ORR) at the cathode side [3].

The main progresses in the cathodic side have been devoted to the development and improvement of activity and stability of non-platinum materials, such as heat-treated macrocyclic compounds of transition metals [4-6], ruthenium based chalcogenides [7-9] and palladium alloys catalysts [10-12]. The last being the most promising alternatives, due to lower price and higher Pd mining sources in comparison with platinum. Besides Pd being cheaper ($654.1 per oz.) than Pt ($1796.9 per oz.) [13], the addition of other metals can increase its activity towards the ORR, in a similar way to the Pt-M catalysts. This increase is caused by the modification of the Pd electronic structure [14], an effect related to the oxygen dissociative adsorption energy. This effect has been reported for 1 nm M@Pd core-shells, which have shown that surface strain and charge distribution can change the Pd shell *d*-band energy [15].

Into the research of Pd alloys, some authors focused their attention in the Pd:Ni alloy. Li *et al* prepared palladium–nickel alloys supported on carbon, observing lower onset potentials and higher ORR activities than those of a Pd/C catalyst in alkaline media [16]. Ramos-Sánchez *et al* focused their research into the catalysts metal loading, preparing bimetallic PdNi nanoparticles supported on carbon by borohydride reduction in a THF solution. These electrocatalysts were also tested as cathode in a PEM fuel cell, finding power densities near 122 mW cm^{-2} for a 45 % metal loading [17]. Previously, the same authors reported higher activity on Pd-Ni catalysts compared to Pd materials, showing a shift in the onset potential for ORR close to 110 mV towards more positive values [18]. Unsupported Pd-Ni catalysts have also been prepared and tested towards

ORR. Xu *et al* [19] de-alloyed a PdNiAl composite, forming a Pd-Ni alloy with uniform and interconnected structure, which displayed both high activity towards the oxygen reduction reaction and higher tolerance to methanol crossover than a Pt/C catalyst in acidic media. Wang *et al* [20] reported the synthesis of Pd-Ni hollow nanoparticles by galvanic replacement, employing Ni nanoparticles as sacrificial electrodes. These materials exhibited better performances towards the oxygen reduction reaction compared to Pt and Pd carbon supported catalysts in alkaline media.

If Pd-Ni nanoparticles are supported on carbon materials, the role of the support and the content and nature of surface functional groups must be considered, when the catalytic activity is assessed. Surface oxygen groups assist the impregnation of metal precursors on the carbon support during the synthesis process [21] and promote the electron transfer between metal particles and the carbon material [22]. In the case of surface nitrogen groups, formation of small size nanoparticles with low sintering degree in presence of these groups has been reported, resulting in more stable catalysts [23].

In this work Pd-Ni catalysts supported on different chemically treated carbon nanofibers have been synthesized, obtaining similar metal contents (close to 25 wt. %) and Pd:Ni atomic ratios close to 1:2, in order to evaluate their catalytic activity towards the oxygen reduction reaction, as an alternative to platinum electrocatalysts for oxygen reduction reaction. The synthesized catalysts were analyzed by EDX, XRD and TEM for determining their physical and morphological properties (composition, size and dispersion of the nanoparticles on carbon supports) whereas an electrochemical study with RRDE techniques was perform in order to evaluate the catalytic activity of synthesized materials at 20 ºC towards the oxygen reduction reaction.

2. EXPERIMENTAL

2.1 Carbon nanofibers

Carbon nanofibers (CNFs) were prepared by catalytic thermal decomposition of methane [24] on a Ni:Cu:Al catalyst (atomic ratio = 78:6:16) at 700 ºC for 10 h [25]. Then, CNFs were treated in HNO_3 65% (v/v) for 2 h at 110 ºC, in order to create surface oxygen groups (carbon support here named as CNFO) and remove the metals used in the synthesis (Ni, Al and Cu) [26]. Nitrogen surface groups on carbon nanofibers were

generated mixing CNFO with ethylenediamine, 10:6 molar ratio, at room temperature for 24 h. Then, the new carbon material (here named as CNFN) was washed to pH 7.0 and dried at 85 ºC for 24 h.

2.2 Preparation of Pd-Ni catalysts

The modified carbon materials were well-dispersed in ultra-pure water by sonication and magnetic stirring. Next, a solution of the precursor salts (Na_2PdCl_4, 98 wt. %, $NiCl_2$, 99.999 wt. %, Aldrich) was slowly added to the dispersion and then, pH was adjusted to 5.0 with a concentrated NaOH solution (98 %, Panreac). After 12 h, a 26.4 mM sodium borohydride solution (99 %, Aldrich) was added drop by drop under sonication. Reaction mixture was kept under magnetic stirring for 12 h, before the filtering, washing and drying at 60 ºC. Nomenclature of the synthesized catalysts depends on the carbon support and the Pd:Ni atomic ratio, labeling them as Pd-Ni/CNF 1:2, Pd-Ni/CNFO 1:2, Pd-Ni/CNFN 1:2 and Pd-Ni/CB 1:2.

Additionally, carbon black (Cabot®) was employed for preparing a Pd:Ni 1:2 catalyst, which was used as a comparison. A commercial Pd/C from E-TEK was also used as a standard.

2.3 Physical characterization

Metal content and Pd-Ni atomic ratios for the synthesized materials were determined by energy dispersive X ray analysis (EDX) using a scanning electron microscope Hitachi S-3400 N coupled to a Röntec XFlash analyser, operating at 15 keV, with a Si(Li) detector and a Be window.

A Bruker AXS D8 Advance diffractometer was employed for obtain the X-ray diffraction (XRD) patterns. This equipment works with a θ-θ configuration and a Cu-Kα radiation at 40 kV and 40 mA. Scans were collected at 1^o min^{-1} for 2θ values between 10 and 100^o.

Analyses of the dispersion and particles size distribution were performed by transmission electron microscopy analysis (TEM). A transmission electron microscope 200 kV JEOL-2000 FXII was employed. Images were obtained by means of a MultiScan CCD (Gatan 694) camera, and they were treated with the Fourier Transform

software Digital Micrograh (3.7.0, Gatan) for obtaining the particle size distribution histograms.

2.4 Electrochemical characterization

An AUTOLAB NS 85630 modular equipment connected to a three electrodes cell was used for carry out the potentiostatic measurements. Working electrode was a glassy carbon disk modified with the Pd-Ni catalysts. It was prepared from an ink containing 2.0 mg of catalyst, 15 µL of Nafion® (5 wt. %, Aldrich) and 500 µL of ultra-pure water; then, a 60 µL aliquot was deposited and dried on the glassy carbon disk. As counter electrode, a glassy carbon bar was used, whereas a reversible hydrogen electrode (RHE) placed inside a Luggin capillary was used as reference electrode; all potentials presented in the text are referred to this electrode. The supporting electrolyte was 0.1 M KOH (99.99%, Aldrich) solution in high resistivity deoxygenated 18.2 MΩ H_2O. Electrochemical tests for the oxygen reduction reaction were performed employing a Hg/HgO reference electrode placed on a Luggin capillary. For an easier comparison, all the potentials have been converted to RHE. The electrolyte was previously saturated with oxygen (99.999 %, BOC) during 20 min. before each test. Measurements were conducted using a rotating-ring disk electrode (RRDE) operated with an ALS Rotation Controller and an Ivium-CompactStat bipotentiostat. The RRDE consisted of a 4 mm diameter glassy carbon disk and a platinum ring with a 7 mm outer diameter. The final loading onto the electrode was 150 $\mu g_{catalyst}$ cm^{-2}.

3. RESULTS AND DISCUSSION

3.1 Carbon nanofibers characterization

Table 1 shows the textural properties and nitrogen content for the carbon nanofibers and the carbon black employed as supports for the Pd-Ni nanoparticles. Chemical treatment induced an increase in the surface area, pore volume and pore diameter of CNFs, especially in the case of N-modified carbon nanofibers, which overcame the pore diameter exhibited by all the carbon materials. Nonetheless, carbon black showed the biggest value for surface area and pore volume. The chemical treatment of the carbon nanofibers with nitric acid in the experimental conditions previously mentioned possibly induced the creation of different surface oxygen groups,

being some of them carboxylic acids, according to the results reported in other previous works [26, 27]. Therefore, a molecule with basic groups as ethylenediamine can react with the O-modified carbon nanofibers. This fact was evidenced in the nitrogen content increase for the CNFN material, which suggests that the chemical treatment of CNFO with ethylenediamine induced the successful incorporation of nitrogen in the carbon material in form of surface nitrogen groups [28, 29].

3.2 Physical characterization

Metal content and Pd:Ni atomic ratios for the Pd-Ni/C catalysts were determined by EDX analysis and the data are reported in Table 2. The values were close to the nominal ones expected from the synthesis procedure (25 wt. % and 1:2, respectively). XRD patterns of the studied materials (Figure 1) exhibited signals attributed to the well-known Pd face-centered cubic structure. Peaks were located at 40º, 47º, 68º and 82º, corresponding to the Pd (111), (200), (220) and (311) facets, respectively [30]. The low intensity of these signals indicates a relatively low crystallinity degree. Previous works in the literature observed that as a consequence of the nickel presence, the particle size decreases and thus, the amount of crystalline facets [31]. Moreover, the presence of crystalline β-$Ni(OH)_2$ was evidenced from the peak located at ~20º, which corresponds to the reflection of the (001) facet for this specie [32]. In the case of the materials supported on CNFs, an intense peak close to 25º was observed, which corresponds to the C(002) graphite basal planes [33, 34]. The intensity of this peak can be explained from the bigger amount of graphitic planes present in CNFs compared to Vulcan.

TEM images of the materials are showed in Figure 2. As a general trend, the catalysts supported on CNFs display particle sizes between 3.4 and 4.1 nm, bigger than that observed for the nanoparticles supported on Vulcan (Pd-Ni/CB 1:2). In fact, the histograms for these materials present a wider range of diameters than that obtained for the catalyst Pd-Ni/CB. Nevertheless, the nanoparticles supported on chemical-modified carbon nanofibers presented lower average particle diameters than those supported on the carbon nanofibers without any chemical treatment, suggesting that presence of surface oxygen and nitrogen groups promotes the formation of smaller size particles. This effect was also evident in the dispersion of the nanoparticles on the different

carbon supports, considering a negligible formation of aggregates on CNFO and CNFN carbon supports.

3.3 Oxygen reduction reaction (ORR) on the synthesized catalysts

Figure 1SI shows the results obtained for the electrochemical characterization of the catalysts in the support electrolyte. Typical signals for the hydrogen adsorption-desorption processes were observed between 0 and 0.3 V *vs* RHE in all the studied materials, whereas the formation/reduction of Pd oxides can be seen in the 0.7 – 1.0 V. The oxygen electrochemical reduction (ORR) on the synthesized Pd-Ni catalysts was studied and Figure 3 presents the results obtained for RRDE experiments at 1600 rpm. Top panel displays the current density at the Pt-ring (j_{RING}) and the botton panel at the disk (j_{DISK}), the area used to normalize the currents was the geometric area of the disk.

The first obvious observation is that the catalysts supported on CNFs displayed similar onset potentials, with values close to 0.98 V *vs* RHE. This onset potential falls within the range of values reported in the literature for Pd-Ni alloys in alkaline media [35]. It also needs to be mentioned, that the onset potential for the CNFs used as supports (as shown in Figure 2SI) occurs at more negative potentials, confirming the involvement of the Pd-Ni sites in the reaction. On the other hand, the onset value for the catalyst Pd/C E-TEK was close to 1.04 V, resulting in a difference of 60 mV. This observation suggests that the commercial Pd catalyst is more active toward ORR, however, it needs to be considered the lower Pd content in the Pd-Ni alloys.

It is interesting to see that the magnitude of the ring (j_{RING}) and disk (j_{DISK}) current densities for the different electrodes is affected by the nature of the carbon nanofibers used as support. Pd-Ni/CNF and Pd-Ni/CNFN catalysts exhibited high diffusional current densities for the oxygen reduction and low currents at the ring, suggesting a low production of hydrogen peroxide. In the case Pd-Ni/CNFO the lowest diffusional current densities and the highest production of hydrogen peroxide were found. It is possible that oxygen surface groups promote the production of this intermediate, a behavior corroborated from the ORR experiments performed on the employed carbon supports (Figure 2SI in supplementary information), which

demonstrated high current densities at the ring and low diffusion current densities for the oxygen reduction on CNFO.

By using the current values recorded at the disk and ring electrodes at 1600 rpm, the H_2O_2 yield was calculated and is shown in Figure 4. The catalysts Pd-Ni/CNF and the commercial Pd/C E-TEK displayed the lowest production percentage, with values below 20%. On the other hand, Pd-Ni/CNFO and Pd-Ni/CNFN showed higher hydrogen peroxide production percentages, suggesting that the oxygen and nitrogen groups, somehow, promote the formation of this intermediate during the oxygen reduction. This result is in agreement with some reports in literature, that demonstrated an increase in the production of hydrogen peroxide during the ORR on N-doped and non-reduced graphene oxide quantum dots [36], N-doped graphenes [37] and graphitic-based materials (highly oriented pyrolytic graphite and glassy carbon) with quinones, anthraquinones and hydroquinones as surface functional groups [38, 39]. This behavior is also reflected when calculating the number of electrons transferred during the reaction (see blue lines in Figure 4). In the case of Pd-Ni/CNF and Pd/C E-TEK, the number of transferred electrons was close to 4 in all the potential range. For Pd-Ni/CNFO and Pd-Ni/CNFN values close to 3.5 electrons were observed, indicating changes in the reaction mechanism, principally related to a contribution from the reduction of oxygen to hydrogen peroxide (as called indirect pathway). Li *et al* proposed a relation between the number of transferred electrons and the Pd:Ni ratios of the catalysts, showing a decrease in the number of electrons with the increase of Ni in the formed alloy. This behavior was explained from the presence of a high amount of Ni atoms on catalyst surface and their participation in the addressing of the reaction mechanism towards the formation of hydrogen peroxide [16].

Figure 5 shows the Koutecky-Levich plots analysis, in order to identify the possible reduction pathways associated with the different materials. The catalyst Pd-Ni/CNFO showed no parallel trends at the different studied potentials, suggesting the existence of a 2+2 mechanism in the oxygen reduction and strengthen the above postulated argument, which makes reference to the production of hydrogen peroxide promoted by surface oxygen groups. These deviations from the parallelism were also observed in the Koutecky-Levich plots for the CNFO carbon support, reported in the

Figure 6SI of the supplementary information. The other materials presented trends close to the parallelism, as a proof of a four electron process and thus, a direct reduction of oxygen to water.

Finally, an interesting point to assess is the performance of the different catalysts against each other. Benchmarking of ORR processes is not straight forward, in order to compare the activity of different electrocatalysts it is common to take the kinetically controlled current density, where influences of mass transport are negligible [40, 41]. Catalytic activities of the different electrodes are compared in Table 3, where kinetic currents at 0.85 V were calculated. Table 3 shows a value which is up to nine times bigger for the commercial catalyst than for some of the synthetized Pd-Ni materials, which reflect the difference in the current-potential relationship between the pure Pd commercial and the Pd-Ni catalysts. However, it should be considered that the Pd loadings are significantly different. Normalizing i_k(0.85 V) by the Pd loading, we estimated a value of $9.8 \cdot 10^{-5}$ A μg^{-1} for Pd-Ni/CNFO, revealing that the Pd sites in the Pd-Ni samples are significantly more active than in the commercial catalysts, suggesting an improvement of the activity with the addition of Ni. It is possible to compare the obtained i_k values con some reported in literature. Zhao *et al* [42] reported maxima i_k(0.7 V) values, normalized by the metal loading, close to $1.0 \cdot 10^{-4}$ A μg^{-1}, for $Pd_{80}Ni_{20}$/C catalysts supported on Vulcan XC-72R carbon black, with a metal loading close to 20 wt. %. The authors also reported the effect of the heat treatment of the catalysts at 500, 700 and 900 ºC, which caused a decrease of the i_k(0.7 V) with the increase of temperature. Wang *et al* [20] reported the synthesis of PdNi hollow nanoparticles with different Pd:Ni ratios, observing a decrease in the i_k(−0.114 V (vs Ag/AgCl)), between $3.05 \cdot 10^{-7}$ A μg^{-1}_{Pd} and $1.84 \cdot 10^{-7}$ A μg^{-1}_{Pd}, with the increase of the atomic Pd ratio from 0.5 and 3. The authors also reported i_k values close to $1.51 \cdot 10^{-7}$ A μg^{-1}_{Pt} and $1.62 \cdot 10^{-7}$ A μg^{-1}_{Pd} for Pt/C and Pd/C catalysts, respectively, explaining the high i_k values determined for the PdNi catalysts to the changes in the surface electronic properties of Pd with the addition of Ni. Considering the i_k values here reported for the Pd-Ni catalyst supported on carbon nanofibers, it is possible to suggest that these materials can be employed as cathodes in direct methanol fuel cells.

4. CONCLUSIONS

Pd-Ni catalysts supported on carbon nanofibers were synthesized, with metal loadings and Pd:Ni atomic ratios close to 25 wt. % and 1:2, respectively. XRD patterns evidenced low crystallinity for these materials, whereas TEM analyses showed a good dispersion of the nanoparticles on the carbon support. The electrochemical characterization of the studied catalysts in the support electrolyte demonstrated that carbon supports affect the catalytic activity in both, the hydrogen adsorption – evolution process, the capacitive currents and the formation of Pd oxides.

Similar onset potentials for ORR were observed for the synthetized Pd-Ni catalysts, although these were still 60 mV shifted to more negative potentials than the Pd/C E-TEK commercial catalyst. Some differences were appreciated in terms of the hydrogen peroxide formed as intermediate in this reaction. Pd-Ni/CNF and Pd/C E-TEK showed the lower production of this intermediate, whereas Pd-Ni/CNFO displayed the highest current densities associate to the production of this intermediate, indicating that oxygen surface groups induce the formation of hydrogen peroxide, principally between 0.5 - 0.7 V *vs* RHE. The ORR on the other synthesized catalysts and the commercial is addressed predominantly towards the formation of water, in agreement with the Koutecky-Levich analysis. To account for the different Pd content, i_k at 0.85 V was normalized in terms of mass. In this sense, higher i_k values normalized by Pd mass at 0.85 V were found, in comparison with the observed value for Pd/C E-TEK. From the results presented in this work, it is possible to suggest the use of Pd-Ni catalysts supported on carbon nanofibers as cathodes in direct methanol fuel cells.

ACKNOWLEDGEMENTS

The authors gratefully acknowledge financial support given by Spanish MINECO (ENE2014-52518-C2-1-R). UK Catalysis Hub is kindly thanked by VC and DJF for resources and support provided via our membership of the UK Catalysis Hub Consortium and funded by EPSRC (grants EP/K014706/1, EP/K014668/1, EP/K014854/1, EP/K014714/1 and EP/M013219/1).

REFERENCES

[1] Wang ZB, Yin GP, Shi PF. Effects of ozone treatment of carbon support on Pt-Ru/C catalysts performance for direct methanol fuel cell. Carbon 2006;44:133-40.

[2] Zhang J, Tang S, Liao L, Yu W. Progress in non-platinum catalysts with applications in low temperature fuel cells, Chinese J Catal 2013;34:1051-65.

[3] Gasteiger HA, Kocha SS, Sompalli B, Wagner FT. Activity benchmarks and requirements for Pt, Pt-alloy and non-Pt oxygen reduction catalysts for PEMFCs. Appl Catal B-Environ 2005;56:9-35.

[4] Baranton S, Coutanceau C, Roux C, Hahn F, Leger JM. Oxygen reduction reaction in acid medium at iron phthalocyanine dispersed on high surface area carbon substrate: tolerance to methanol, stability and kinetics. J Electroanal Chem 2005;577:223-34.

[5] Wagner AJ, Wolfe GM, Fairbrother DH. Reactivity of vapor-deposited metal atoms with nitrogen-containing polymers and organic surfaces studied by in situ XPS. Appl Surf Sci 2003;219:317-28.

[6] Matter PH, Zhang L, Ozkan US. The role of nanostructure in nitrogen-containing carbon catalysts for the oxygen reduction reaction. J Catal 2006;239:83-96.

[7] Serov AA, Min M, Chai G, Han S, Kang S, Kwak C. Preparation, characterization and high performance of RuSe/C for direct methanol fuel cells. J Power Sources 2008;175:175-82.

[8] Zaikovskii VI, Nagabhushana KS, Kriventsov VV, Loponov KN, Cherepanova SV, Kvon RI, Bönnemann H, Kochubey DI, Savinova ER. Synthesis and structural characterization of Se-modified carbon supported Ru nanoparticles for the oxygen reduction reaction. J Phys Chem B 2006;110:6881-90.

[9] Shukla AK, Raman RK. Methanol-resistant oxygen-reduction catalysts for direct methanol fuel cells. Annu Rev Mater Res 2003;33:155-68.

[10] Mustain WE, Kepler K, Prakash J. Investigations of carbon-supported $CoPd_3$ catalysts as oxygen cathodes in PEM fuel cells. Electrochem Commun 2006;8:406-10.

[11] Mustain WE, Prakash J. Kinetics and mechanism for the oxygen reduction reaction on polycrystalline cobalt-palladium electrocatalysts in acid media. J Power Sources 2007;170:28–37.

[12] Serov AA, Cho SY, Han S, Min M, Chai G, Nam KH, Kwak C. Modification of palladium-based catalysts by chalcogenes for direct methanol fuel cells. Electrochem Commun 2007;9:2041-4.

[13] Shao M. Palladium-based electrocatalysts for hydrogen oxidation and oxygen reduction reactions. J Power Sources 2011;196:2433-44.

[14] Wei YC, Liu CW, Wang KW. Improvement of oxygen reduction reaction and methanol tolerance characteristics for PdCo electrocatalysts by Au alloying and CO treatment. Chem Commun 2011;47:11927-9.

[15] Tang W, Henkelman G. Charge redistribution in core-shell nanoparticles to promote oxygen reduction. J Chem Phys 2009;130:194504-10.

[16] Li B, Prakash J. Oxygen reduction reaction on carbon supported palladium-nickel alloys in alkaline media. Electrochem Commun 2009;11:1162-5.

[17] Ramos-Sanchez G, Santana-Salinas A, Vazquez-Huerta G, Solorza-Feria O. Electrochemical impedance study and performance of PdNi nanoparticles as cathode catalyst in a polymer electrolyte membrane fuel cell. J New Mat Electrochem Syst 2010;13:213-7.

[18] Ramos-Sánchez G, Yee-Madeira H, Solorza-Feria O. PdNi electrocatalyst for oxygen reduction in acid media. Int J Hydrogen Energ 2008;33:3596-600.

[19] Xu C, Liu Y, Hao Q, Duan H. Nanoporous PdNi alloys as highly active and methanol tolerant electrocatalysts towards oxygen reduction reaction. J Mater Chem A 2013;1:13542-8.

[20] Wang M, Zhang W, Wang J, Wexler D, Poynton SD, Slade RCT, Liu HK, Jensen BW, Kerr R, Shi D, Chen J. PdNi hollow nanoparticles for improved electrocatalytic oxygen reduction in alkaline environments. ACS Appl Mater Interfaces 2013;5:12708-15.

[21] Van Dam HE, Van Bekkum H. Preparation of platinum on activated carbon. J Catal 1991;131:335-49.

[22] Gallezot P, Richard D, Bergeret G. Low-nuclearity platinum clusters supported on graphite. ACS Symp Ser 1990;437:150-9.

[23] Ott LS, Finke RG. Transition-metal nanocluster stabilization for catalysis: A critical review of ranking methods and putative stabilizers. Coord Chem Rev 2007;251:1075-100.

[24] Suelves I, Lázaro MJ, Moliner R, Corbella BM, Palacios JM. Hydrogen production by thermo catalytic decomposition on methane on Ni-based catalysts: influence of operating conditions on catalysts deactivation and carbon characteristics. Int J Hydrogen Energy 2005;30:1555-67.

[25] Suelves I, Lázaro MJ, Moliner R, Echegoyen Y, Palacios JM. Characterization of NiAl and NiCuAl catalysts prepared by different methods for hydrogen production by thermo catalytic decomposition of methane. Catal Today 2006;116:271-80.

[26] Calvillo L, Lázaro MJ, Suelves I, Echegoyen Y, Bordejé EG, Moliner R. Study of the surface chemistry of modified carbon nanofibers by oxidation treatments in liquid phase. J Nanosci Nanotech 2009;9:4164-9.

[27] Sebastián D, Suelves I, Moliner R, Lázaro MJ. The effect of the functionalization of carbon nanofibers on their electronic conductivity. Carbon 2010;48:4421-31.

[28] Keramati M, Ghoreyshi AA. Improving CO_2 adsorption onto activated carbon through functionalization by chitosan and triethylenetetramine. Physica E 2014;57:161-8.

[29] Lázaro MJ, Alegre C, Nieto-Monge MJ, Sebastián D, Gálvez ME, Pastor E, Moliner R. Nitrogen doped and functionalized carbon materials as supports for catalysts in electro-oxidation of methanol. Adv Sci Tech 2014;93:41-9.

[30] Li R, Wei Z, Huang T, Yu A. Ultrasonic-assisted synthesis of Pd-Ni alloy catalysts supported on multi-walled carbon nanotubes for formic acid electrooxidation. Electrochim Acta 2011;56:6860-5.

[31] Zhang Z, Xin L, Sun K, Li W. Pd-Ni electrocatalysts for efficient ethanol oxidation reaction in alkaline electrolyte. Int J Hydrogen Energ 2011;36:12686-97.

[32] Zhu LP, Liao GH, Yang Y, Xiao HM, Wang JF, Fu SY. Self-assembled 3D flower-like hierarchical β-$Ni(OH)_2$ hollow architectures and their in situ thermal conversion to NiO. Nanoscale Res Lett 2009;4:550-7.

[33] Li W, Liang C, Zhou W, Qiu J, Zhou Z, Sun G, Xin Q. Preparation and characterization of multiwalled carbon nanotube-supported platinum for cathode catalysts of direct methanol fuel cells. J Phys Chem B 2003;107:6292-9.

[34] Jeng K, Chien C, Hsu N, Yen S, Chiou S, Lin S, Huang WM. Performance of direct methanol fuel cell using carbon nanotube-supported Pt-Ru anode catalyst with controlled composition. J Power Sources 2006;160:97-104.

[35] Holade Y, Sahin NE, Servat K, Napporn TW, Kokoh KB. Recent advances in carbon supported metal nanoparticles preparation for oxygen reduction reaction in low temperature fuel cells. Catalysts 2015;5:310-48.

[36] Favaro M, Ferrighi L, Fazio G, Colazzo L, Di Valentin C, Durante C, Sedona F, Gennaro A, Agnoli S, Granozzi G. Single- and multi-doping in graphene quantum dots: unraveling the origin of selectivity in the oxygen reduction reaction. ACS Catal 2015; in press; DOI: 10.1021/cs501211h.

[37] Li Q, Zhang S, Dai L, Li LS. Nitrogen-doped colloidal graphene quantum dots and their size-dependent electrocatalytic activity for the oxygen reduction reaction. J Am Chem Soc 2012;134:18932-5.

[38] Mooste M, Kibena E, Sarapuu A, Mäeorg U, Maia G, Tammeveski K. Electrocatalysis of oxygen reduction on glassy carbon electrodes modified with anthraquinone moieties. J Solid State Electrochem 2014;18:1725-33.

[39] Kocak I, Ghanem MA, Al-Mayouf A, Alhoshan M, Bartlett PN. A study of the modification of glassy carbon and edge basal highly oriented pyrolytic graphite electrodes modified with anthraquinone using diazonium coupling and solid phase synthesis and their use for oxygen reduction. J Electroanal Chem 2013;706:25-32.

[40] Gasteiger HA, Kocha SS, Sompalli B, Wagner FT. Activity benchmarks and requirements for Pt, Pt-alloy, and non-Pt oxygen reduction catalysts for PEMFCs. Appl Catal B 2005;56:9-35.

[41] Paulus UA, Schmidt TJ, Gasteiger HA, Behm RJ. Oxygen reduction on a high-surface area Pt/Vulcan carbon catalyst: a thin-film rotating ring-disk electrode study. J Electroanal Chem 2001;495:134-45.

[42] Zhao J, Sarkar A, Manthiram A. Synthesis and characterization of Pd-Ni nanoalloy electrocatalysts for oxygen reduction reaction in fuel cells. Electrochim Acta 2010;55:1756–65.

Figure captions

Figure 1. XRD patterns of the synthesized Pd-Ni catalysts.

Figure 2. TEM images (left) and histograms for particle size distribution (right) of the synthesized Pd-Ni catalysts: (a-b) Pd-Ni/CNF 1:2, (c-d) Pd-Ni/CNFO 1:2, (e-f) Pd-Ni/CNFN 1:2 and (g-h) Pd-Ni/CB 1:2.

Figure 3. RDE (bottom) and RRDE (top) measurements of the synthesized Pd-Ni catalysts and the commercial Pd/C catalyst at 1600 rpm in 0.1 M KOH with O_2-saturated. Scan rate: 10 mV s^{-1}.

Figure 4. Production percentage of hydrogen peroxide (black line) and number of electrons (blue line) produced on the different catalysts.

Figure 5. Koutecky–Levich plots for RDE results of Pd-Ni catalysts at different potentials.

Supplementary information

Palladium-Nickel Materials as Cathode Electrocatalysts for Alkaline Fuel Cells

J.C. Calderón[a, †], V. Celorrio[b, †], M.J. Nieto-Monge[a], D.J. Fermín[b], J.I. Pardo[c], R. Moliner[a], M.J. Lázaro[a]*

[a]Instituto de Carboquímica (CSIC), Miguel Luesma Castán 4, 50018, Zaragoza, Spain

[b]School of Chemistry, University of Bristol, Cantocks Close, BS8 1TS, Bristol, United Kingdom

[c]Instituto Universitario de Investigación de Ingeniería de Aragón (I3A), Mariano Esquillor s/n, 50018, Zaragoza, Spain

[†]*These authors contributed equally to this work.*

**Corresponding author email address: mlazaro@icb.csic.es*

Figure 1SI presents the cyclic voltammograms for the electrochemical characterization of the catalysts in the support electrolyte. The signals for the hydrogen adsorption-desorption processes were observed between 0 and 0.3 V *vs* RHE, while those corresponding to the formation/reduction of Pd oxides have been seen in the 0.7 – 1.0 V range.

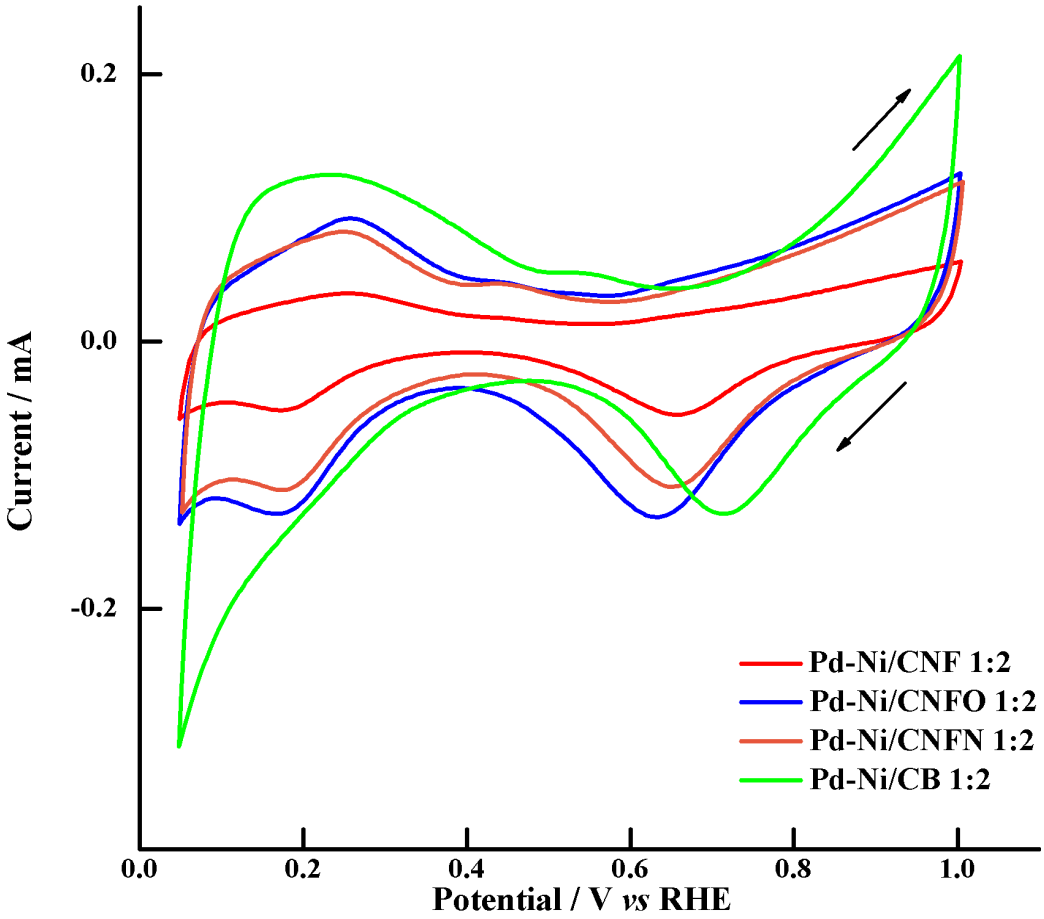

Figure 1SI. Cyclic voltammograms of the synthesized Pd-Ni catalysts in the support electrolyte. Support electrolyte: KOH 0.1 M. Scan rate: 20 mV s^{-1}.

Results obtained for oxygen reduction reaction (ORR) on carbon supports CNF, CNFO, CNFN and CB are presented in Figure 2SI. The onset potentials for the ORR on the carbon supports is notably at more negative potentials than those observed for the Pd-Ni synthesized catalysts, revealing the role of metals in the catalysis for this reaction. Chemical modification of CNFs (*i.e.* CNFO and CNFN) seems to affect these values, shifting the onset potential by 40 mV to more positive potentials compared with the non-chemical treated carbon nanofiber (CNF). Non-modified carbon black showed a 0.78 V onset potential.

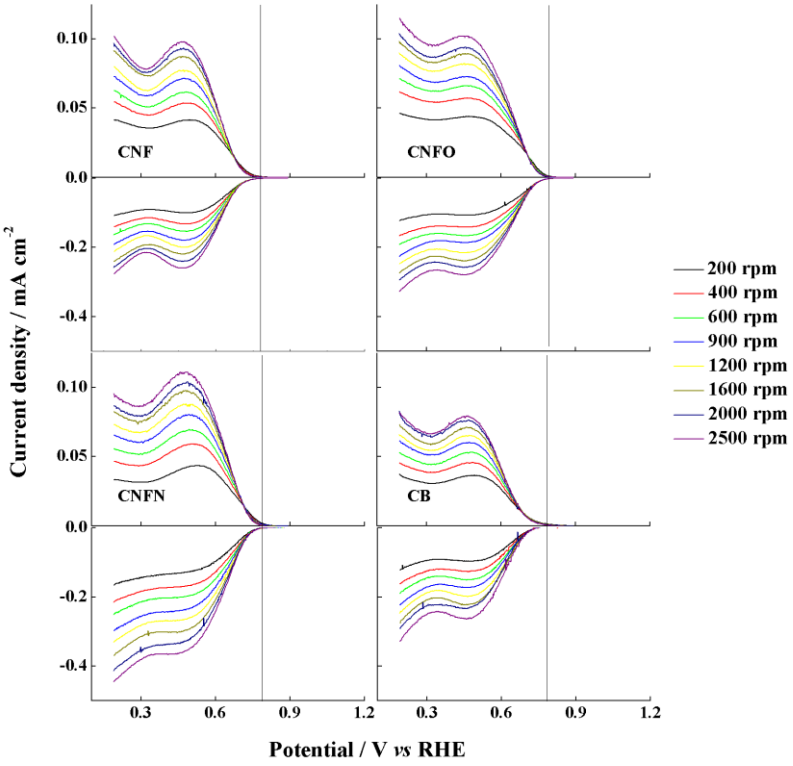

Figure 2SI. Disk measurements (bottom) and ring (top) measurements of the different carbon supports at different rotation rates in 0.1 M KOH with O_2-saturated. Scan rate: 10 mV s^{-1}.

Figure 3SI displayed RRDE experiments at different rotation rates for the samples under study. Higher diffusional current densities were observed for the catalysts Pd-Ni/CNF 1:2 and Pd-Ni/CNFN 1:2. These materials also showed the lowest current densities for the hydrogen peroxide production, whereas the catalyst Pd-Ni/CNFO 1:2 exhibited the lowest diffusional current densities and the highest currents associated to the hydrogen peroxide production.

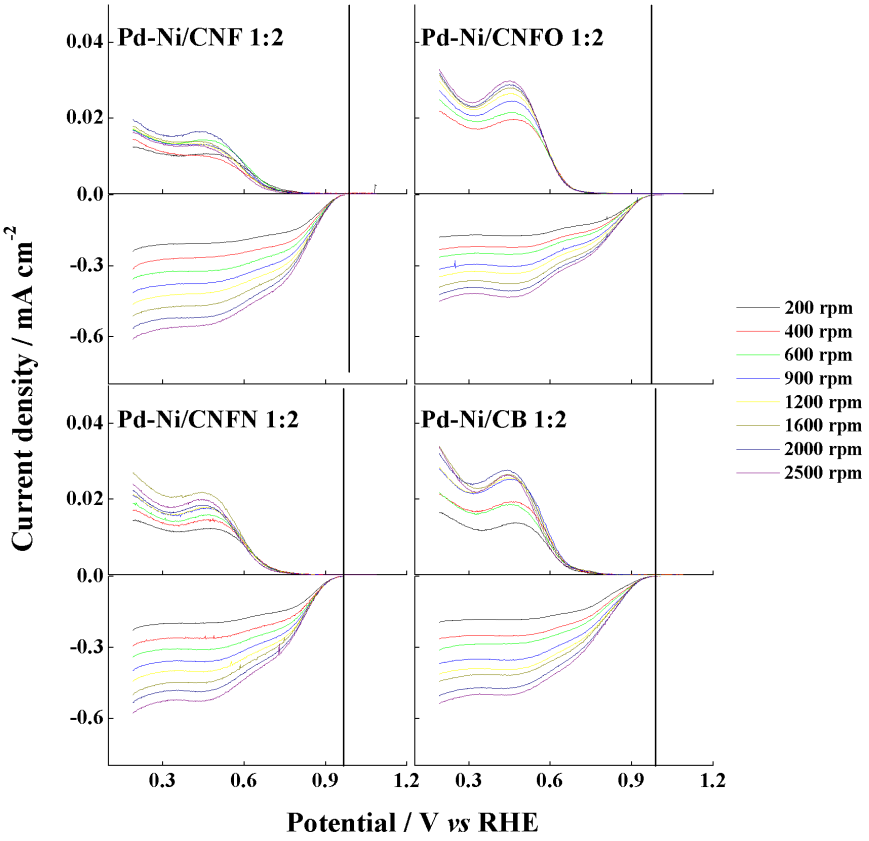

Figure 3SI. RDE measurements (bottom) and RRDE (top) measurements of synthesized Pd-Ni catalysts at different rotation rates in 0.1 M KOH with O_2-saturated. Scan rate: 10 mV s^{-1}.

Figure 4SI shows the hydrogen peroxide production yield when the ORR is performed on the different carbon nanofibers. CNFO showed the high percentages in all the range of applied potentials, whereas CNFN and CB exhibited the lowest values, principally between 0.2 and 0.5 V *vs* RHE.

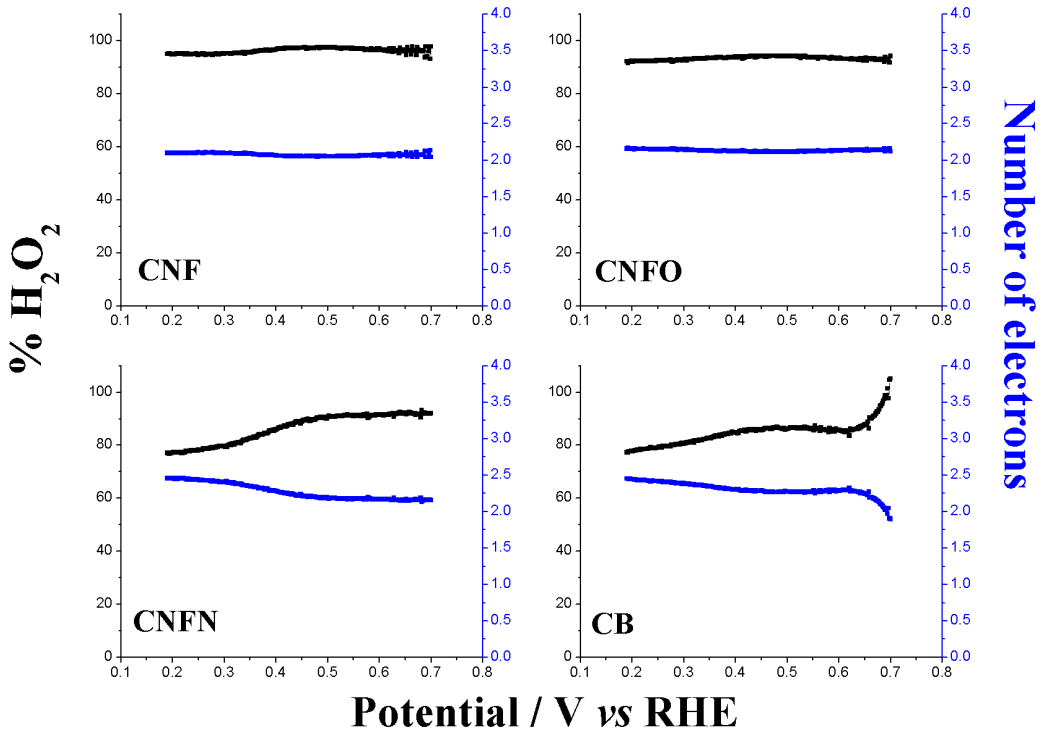

Figure 4SI. Production percentage of hydrogen peroxide (black line) and number of electrons (blue line) produced on the different carbon support.

Figure 5SI shows the RDE and RRDE results for the performance of ORR on the commercial catalyst Pd/C E-TEK, which demonstrated the low production of hydrogen peroxide and the obtaining of high diffusion current densities. The onset for this reaction was at potentials more positive than 1.0 V, as was described in the manuscript.

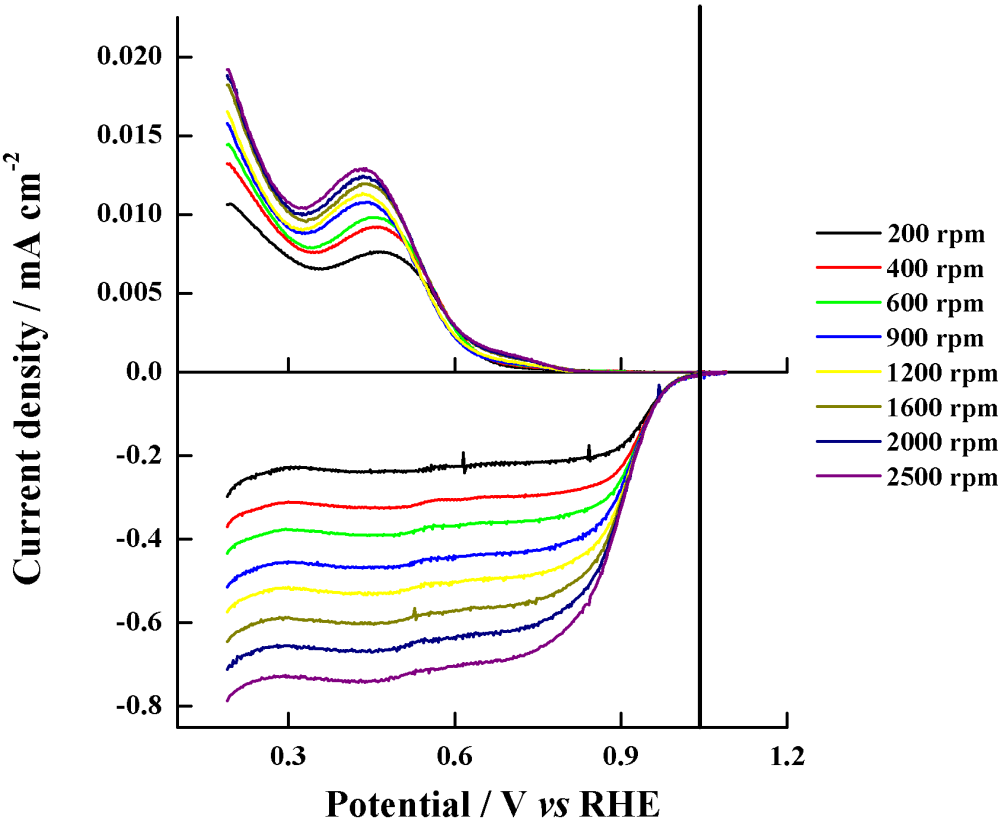

Figure 5SI. RDE measurements (bottom) and RRDE measurements (top) of commercial catalyst Pd/C E-TEK catalysts at different rotation rates in 0.1 M KOH with O_2-saturated. Scan rate: 10 mV s^{-1}.

Koutecky–Levich plots for the carbon materials are presented in Figure 6SI. Deviations from a parallel behavior were observed and suggested the preferential formation of hydrogen peroxide on these materials. The drastic deviations were found for CNF and CB, although the later anchoring of Pd-Ni nanoparticles addressed the ORR mechanism towards the formation of water as final reduction product.

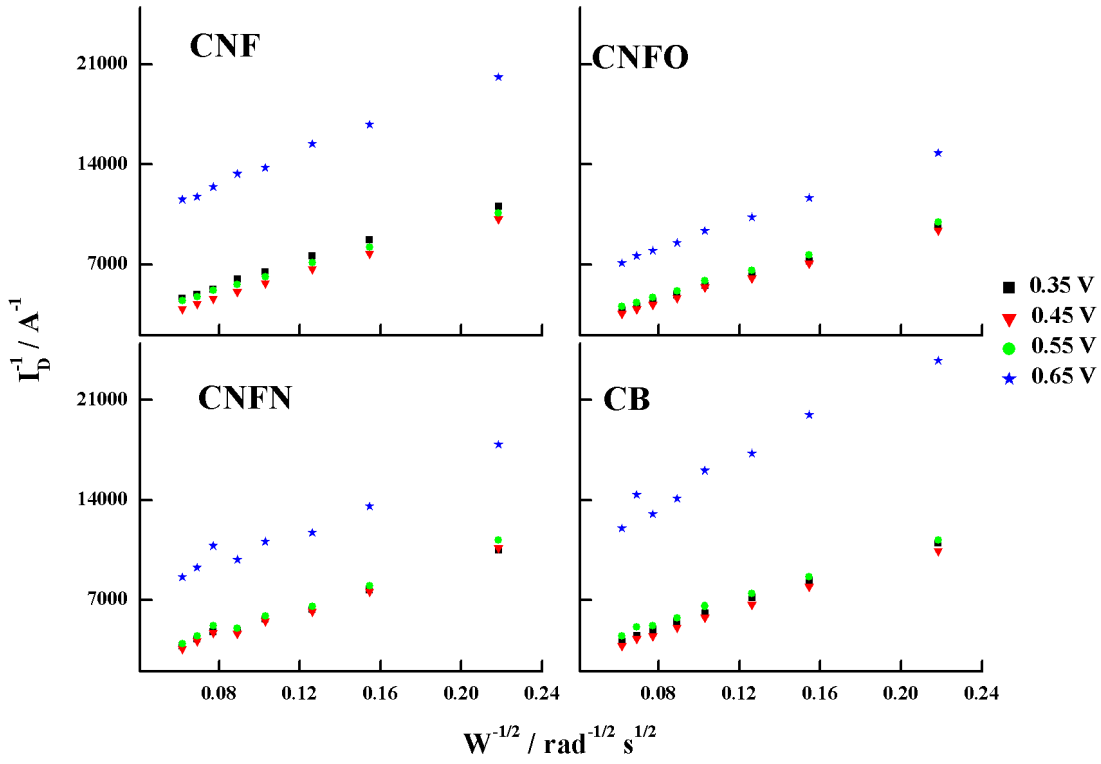

Figure 6SI. Koutecky–Levich plots for RDE results of Pd-Ni catalysts at different potentials.

Table 1. Textural and chemical properties of carbon supports

Carbon supports	**S_{BET} / $m^2\ g^{-1}$**	**V_{total} / $cm^3\ g^{-1}$**	**V_{meso} / $cm^3\ g^{-1}$**	**Pore diameter / nm**	**Nitrogen content / %wt.**
CNF	72.1	0.241	0.239	11.56	0.03
CNFO	72.7	0.260	0.256	11.89	0.13
CNFN	72.5	0.280	0.275	12.63	0.38
CB	214.6	0.412	0.343	9.64	----

Table 2. Physical characterization of synthesized Pd-Ni catalysts.

Catalyst	**Atomic ratio Pd:Ni**	**Metal content / % wt.**	**Pd content / % wt.**	**Ni content / % wt.**	**Particle size / nm**
Pd-Ni/CNF 1:2	33:67	24	12.3	11.8	4.1 $\pm$ 1.2
Pd-Ni/CNFO 1:2	35:65	27	12.0	15.2	3.8 $\pm$ 1.2
Pd-Ni/CNFN 1:2	37:63	18	8.8	9.1	3.4 $\pm$ 1.1
Pd-Ni/CB 1:2	28:72	24	9.8	14.3	2.7 $\pm$ 0.9
Pd/C E-TEK	---	20	20	---	

Table 3. Activity descriptors obtained from the kinetics analysis such as the kinetic current at 0.85 V ($i_{k(0.85)}$) and the kinetic current density by mass of Pd in the electrode ($j_{k(0.85)}$ / A μg^{-1}),

Catalyst	**$i_{k(0.85\ V)}$ / A**	**$j_{k(0.85\ V)}$ / A μg^{-1}**
Pd-Ni/CNF 1:2	$2.1 \cdot 10^{-4}$	$8.8 \cdot 10^{-5}$
Pd-Ni/CNFO 1:2	$2.3 \cdot 10^{-4}$	$9.8 \cdot 10^{-5}$
Pd-Ni/CNFN 1:2	$1.0 \cdot 10^{-4}$	$5.8 \cdot 10^{-5}$
Pd-Ni/CB 1:2	$1.4 \cdot 10^{-4}$	$7.3 \cdot 10^{-5}$
Pd/C E-TEK	$9.4 \cdot 10^{-4}$	$2.4 \cdot 10^{-4}$

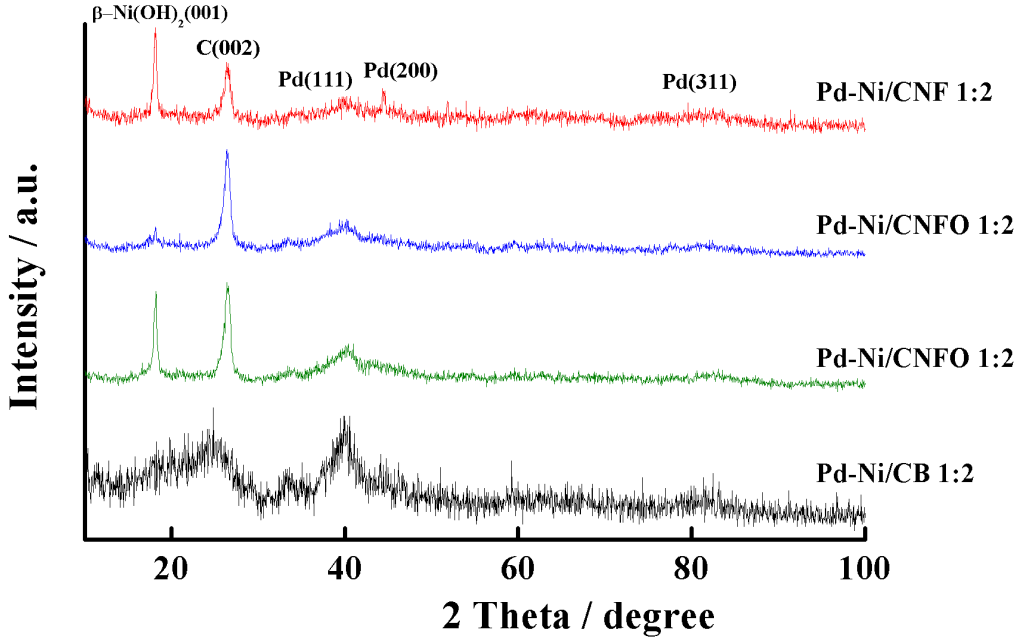
β–Ni(OH)2(001)
C(002)
Pd(111)
Pd(200)
Pd(311)
Pd-Ni/CNF 1:2
Pd-Ni/CNFO 1:2
Pd-Ni/CNFO 1:2
Pd-Ni/CB 1:2
Intensity / a.u.
20
40
60
80
100
2 Theta / degree

Figure 1.

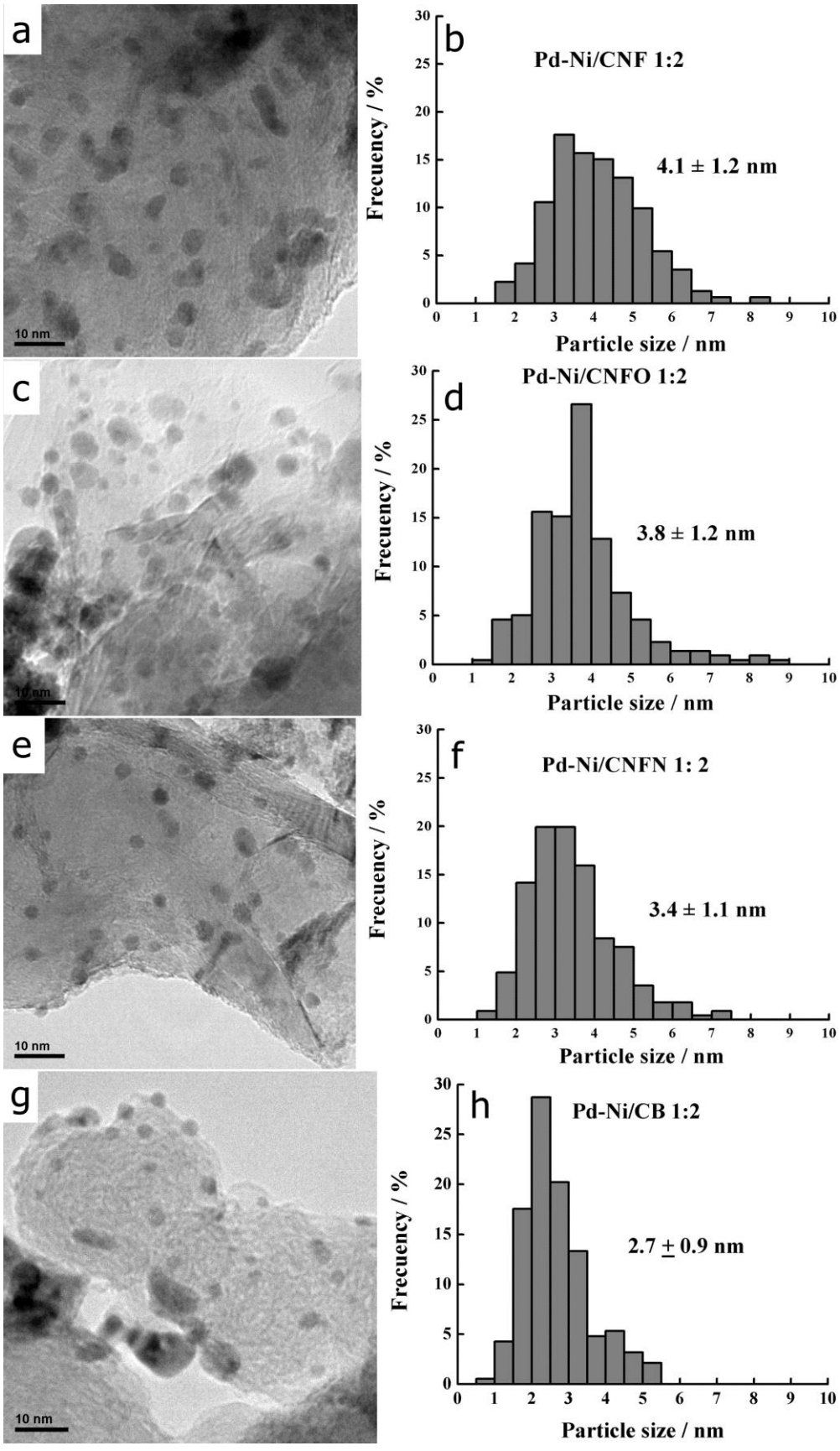
a
10 nm
b
Pd-Ni/CNF 1:2
4.1 ± 1.2 nm
Frecuency / %
Particle size / nm
c
10 nm
d
Pd-Ni/CNFO 1:2
3.8 ± 1.2 nm
Frecuency / %
Particle size / nm
e
10 nm
f
Pd-Ni/CNFN 1: 2
3.4 ± 1.1 nm
Frecuency / %
Particle size / nm
g
10 nm
h
Pd-Ni/CB 1:2
2.7 ± 0.9 nm
Frecuency / %
Particle size / nm

Figure 2.

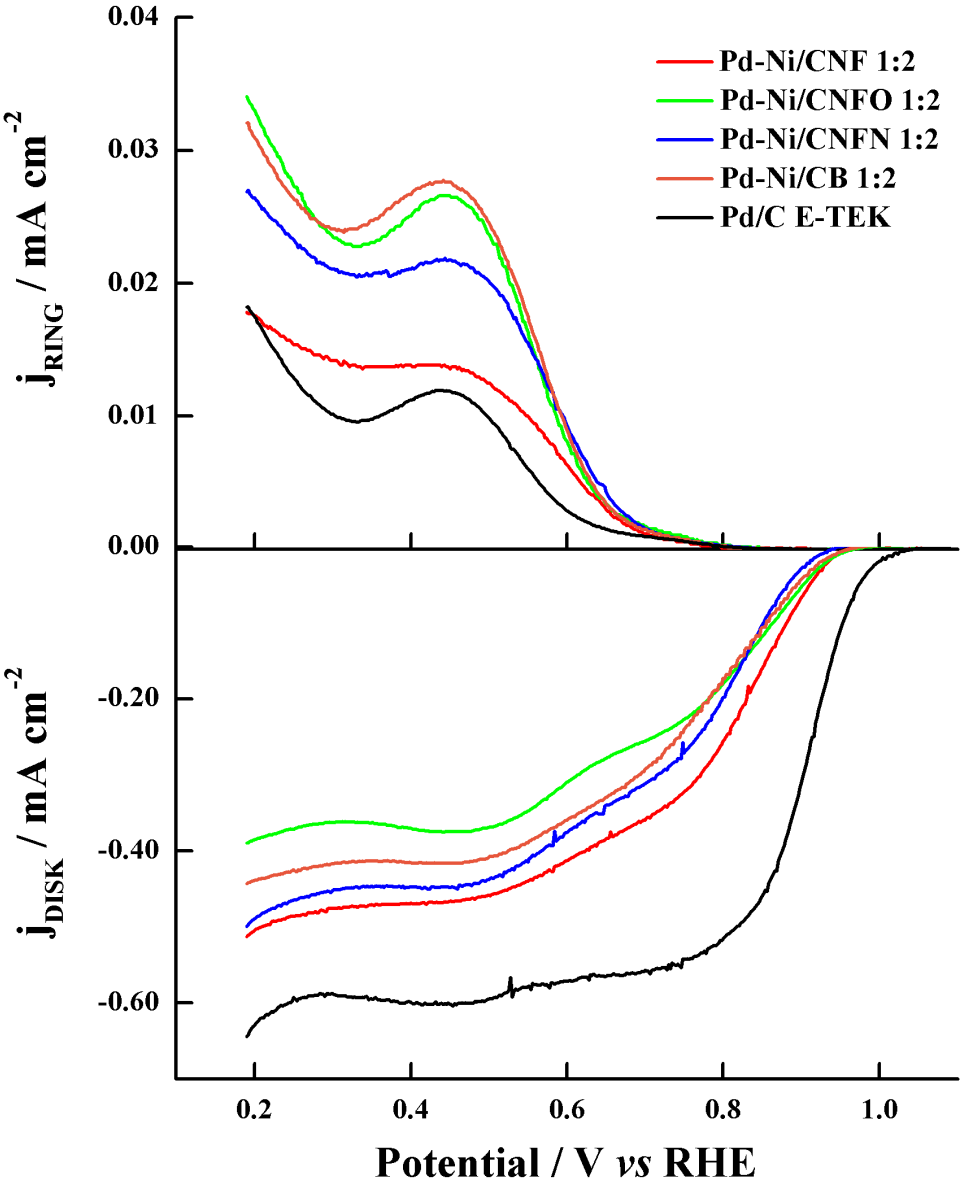
Pd-Ni/CNF 1:2
Pd-Ni/CNFO 1:2
Pd-Ni/CNFN 1:2
Pd-Ni/CB 1:2
Pd/C E-TEK
j_{RING} / mA cm^{-2}
j_{DISK} / mA cm^{-2}
0.04
0.03
0.02
0.01
0.00
-0.20
-0.40
-0.60
0.2
0.4
0.6
0.8
1.0
Potential / V *vs* RHE

Figure 3.

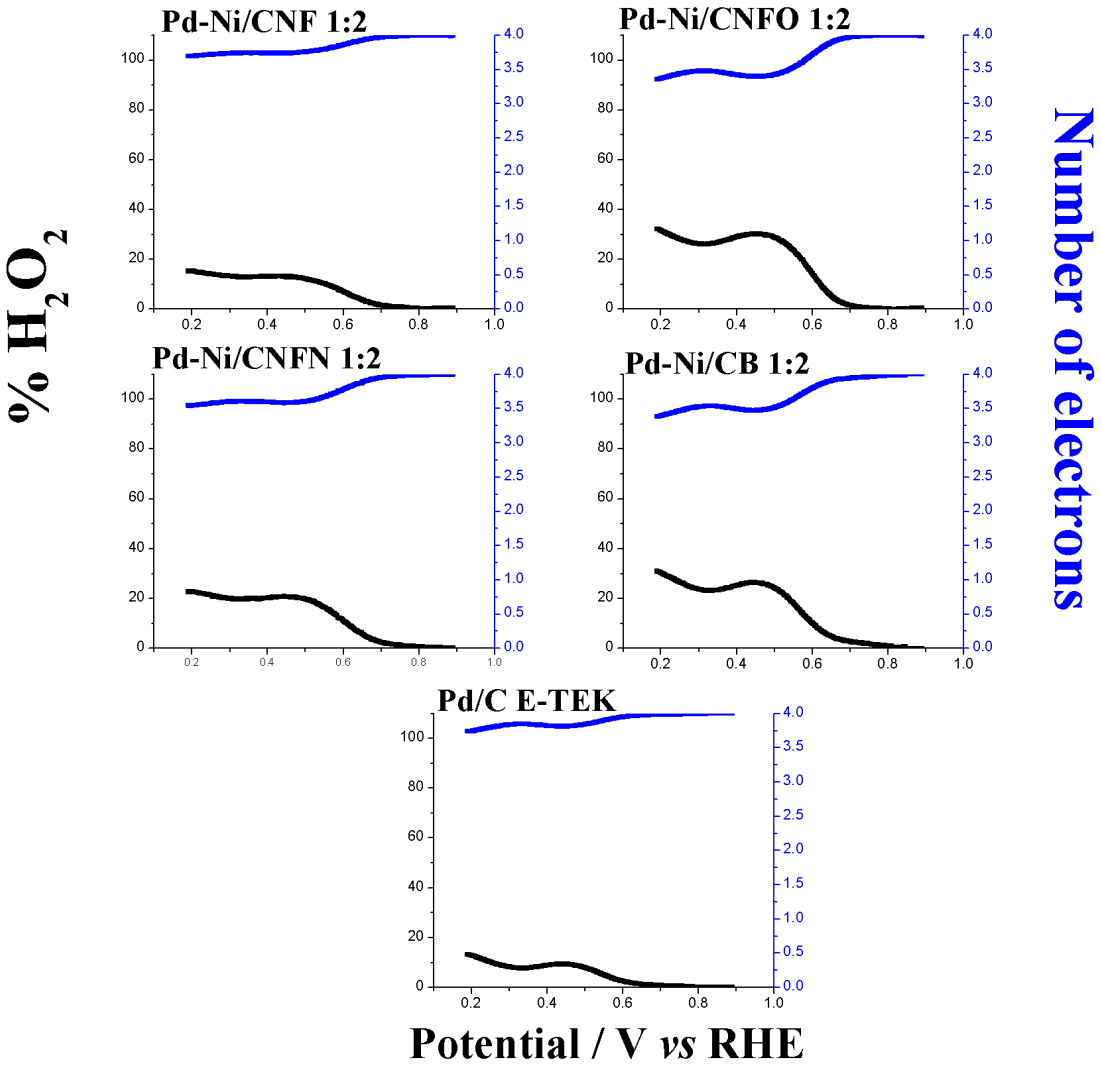
Pd-Ni/CNF 1:2
Pd-Ni/CNFO 1:2
Pd-Ni/CNFN 1:2
Pd-Ni/CB 1:2
Pd/C E-TEK
% H2O2
Number of electrons
Potential / V vs RHE

Figure 4.

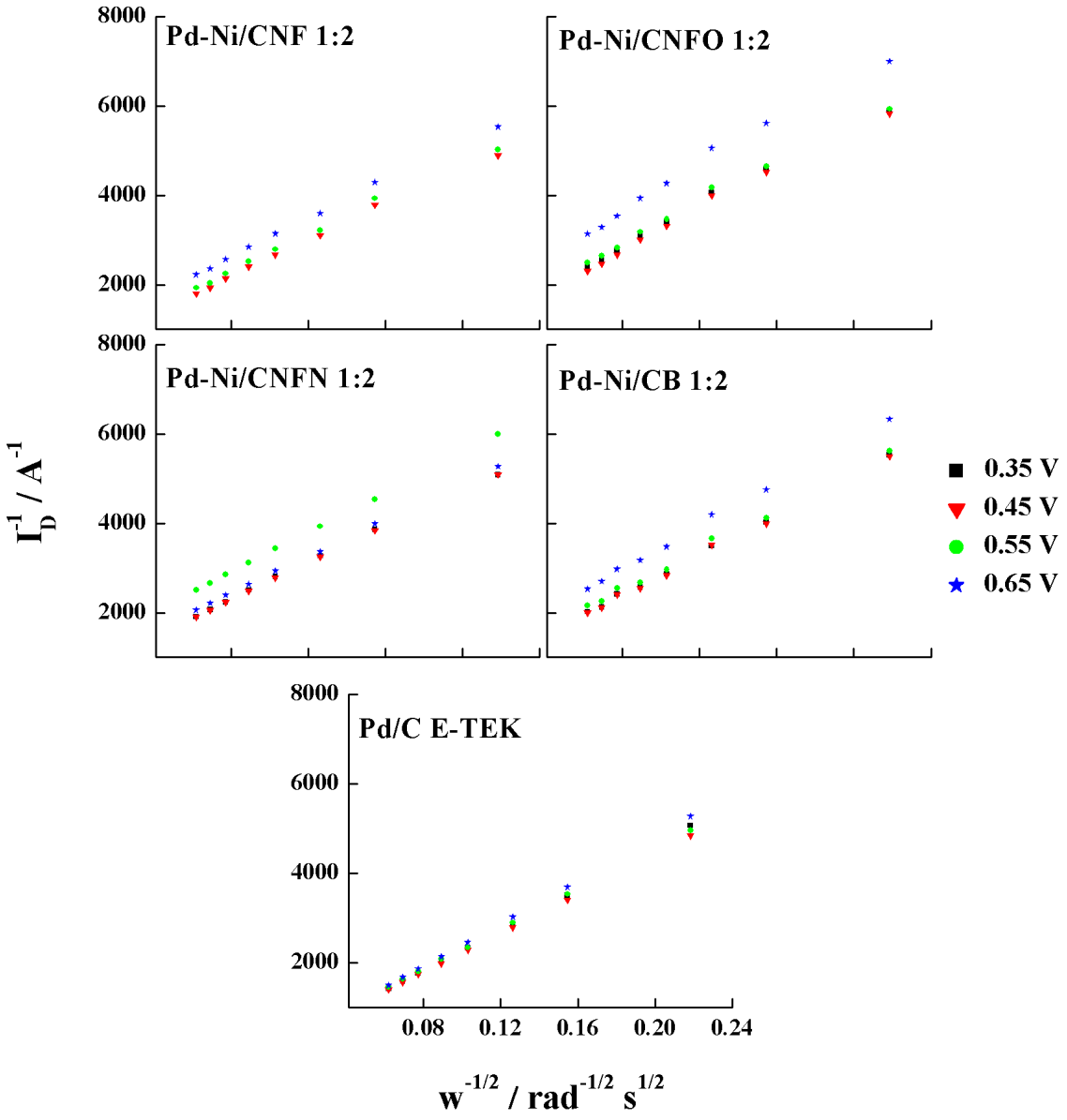
Pd-Ni/CNF 1:2
Pd-Ni/CNFO 1:2
Pd-Ni/CNFN 1:2
Pd-Ni/CB 1:2
Pd/C E-TEK
8000
6000
4000
2000
0.08
0.12
0.16
0.20
0.24
I_D^{-1} / A^{-1}
$w^{-1/2}$ / $rad^{-1/2}$ $s^{1/2}$
0.35 V
0.45 V
0.55 V
0.65 V

Figure 5.